Effect of Composite Stiffened Panel Design on Skin-Stringer Separation in Postbuckling

Kootte, L.J.; Bisagni, C.; Ranatunga, Vipul; Clay, Stephen B.; Dávila, Carlos G.; Rose, Cheryl

DOI
10.2514/6.2021-0441

Publication date
2021

Document Version
Final published version

Published in
AIAA Scitech 2021 Forum

AIAA SciTech Forum
11–15 & 19–21 January 2021, VIRTUAL EVENT
AIAA Scitech 2021 Forum

10.2514/6.2021-0441

Effect of Composite Stiffened Panel Design on Skin-Stringer Separation in Postbuckling

Lucas J. Kootte[1], Chiara Bisagni[2]
Delft University of Technology, Delft, 2629HS, Netherlands

Vipul Ranatunga[3], Stephen B. Clay[4]
Air Force Research Laboratory, Wright-Patterson AFB, Dayton, OH 45433, USA

Carlos G. Dávila[5], Cheryl Rose[6]
NASA Langley Research Center, Hampton, VA 23692, USA

To design aeronautical composite multi-stringer panels that can safely operate in a postbuckled state, it is important to identify the parameters that can influence the different modes in which skin-stringer separation might occur. A methodology is under development to study the interaction between the skin-stringer separation and the postbuckling deformation using the building block approach and single-stringer specimens. In particular, the methodology can identify whether the skin-stringer separation occurs due to bending or twisting, so that these two possible modes can be studied separately. For bending, a simple criterion that can predict the location of initiation is presented. This procedure has the potential to reduce the overall development cost and allows the investigation of the design parameters that influence the skin-stringer separation.

I. Introduction

In the process of designing multi-stringer composite panels for aerospace structures, the possibility of skin-stringer separation is a significant failure concern, especially if the functional requirements have to be satisfied under postbuckled conditions. Design parameters such as structural geometry and dimensions may have a significant effect on the skin-stringer separation. As an example, a change in stringer spacing or stacking sequence can alter the postbuckling deformation and cause a significantly different strain distribution on the panel. Additionally, other factors such as geometric imperfection of the panel [1] or the conditions that affect the interlaminar normal stresses along the flange edge can delay the separation [2] as well.

The interlaminar properties that are important in predicting skin-stringer separation are often determined at the coupon level and are relatively simple to obtain. However, exploring skin-stringer separation in a multi-stringer panel through finite element analyses with cohesive elements or the virtual crack closure technique (VCCT) requires many hours of engineering time and expertise to develop the models and significant computational resources to execute the analyses. A validated simple failure criterion that can be used to predict the initiation of skin-stringer separation would offer significant computational advantages. However, failure criteria to predict the skin-stringer separation have not been the subject of extensive investigation. The Royal Netherlands Aerospace Centre (NLR) proposed a failure criterion that depends on the running loads and moments along the stringers of a panel [3]. This criterion was developed using the seven-point bending test, which was introduced by the NLR [4]. The criterion relies on loads and moments calculated using the classical laminate theory with the assumption of no shear strain at the skin-stringer

[1] PhD Student, Faculty of Aerospace Engineering, AIAA Student Member.
[2] Professor, Faculty of Aerospace Engineering, AIAA Associate Fellow.
[3] Senior Research Engineer, Aerospace Systems Directorate, AIAA Senior Member.
[4] Principal Research Engineer, Aerospace Systems Directorate, AIAA Associate Fellow.
[5] Senior Aerospace Research Engineer, Durability, Damage Tolerance, and Reliability Branch, AIAA Member.
[6] Senior Aerospace Research Engineer, Durability, Damage Tolerance, and Reliability Branch, AIAA Member.

interface. However, only a limited amount of data is available from this study, which was mainly focused on the bending of the skin. An alternative study of Cosentino and Weaver [5] showed an analytical method to obtain the out-of-plane behavior of a postbuckled stiffened panel, specifically focusing on stringer runout locations. Additionally, a fracture mechanics approach was applied to predict debonding of the skin and stringer. Another study was conducted by Falzon et al. [6], who proposed an initiation criterion for delamination at the mid-plane of a T-stringer web subjected to high shear stresses resulting from combined twisting moment and shear loads. Although the focus of this criterion was not on skin-stringer separation, it considered the failure that might occur in the regions experiencing higher twisting. It has been shown previously that the skin-stringer separation in multi-stringer panels can occur in the regions of high twisting or high bending [7-8]. Consequently, it is important to consider both regions and study the critical region in more detail.

A methodology is currently under development to study the interaction between the skin-stringer separation and the postbuckled shape of multi-stringer panels using single-stringer specimens [9]. This paper investigates the initiation of skin-stringer separation using an analytical approach. This approach uses the moment output from a finite element analysis in order to identify the locations of maximum bending and maximum twisting. Subsequently, a failure index is calculated in order to estimate the applied displacement where the stringer will start to separate from the skin due to the postbuckling deformations. Following the methodology [9], a representative single-stringer specimen is designed that can be used to verify the initiation of skin-stringer separation as well as to study the skin-stringer separation in more detail, numerically and experimentally. It is believed that an accurate prediction of the interaction between the skin and stringer leads to a better understanding of the effects of design parameters on skin-stringer separation modes.

II. Methodology

Design of aeronautical composite multi-stringer panels that can safely operate in a postbuckled state is a challenging task because of the complexity of failure modes of the composite materials as well as the interaction between the skin-stringer separation and postbuckling shapes. Due to the geometric complexity and size of such components, it is time consuming and expensive to manufacture and test the number of multi-stinger panels required to satisfy the certification criteria. The problem is compounded by the need to analyze different panel configurations, layups, thicknesses, loading and boundary conditions. Developing finite element models and conducting analyses to predict the failure of multi-stringer components is also time consuming and expensive. In order to reduce the experimental and computational costs, a methodology is proposed, and a flow diagram is reported in Fig. 1.

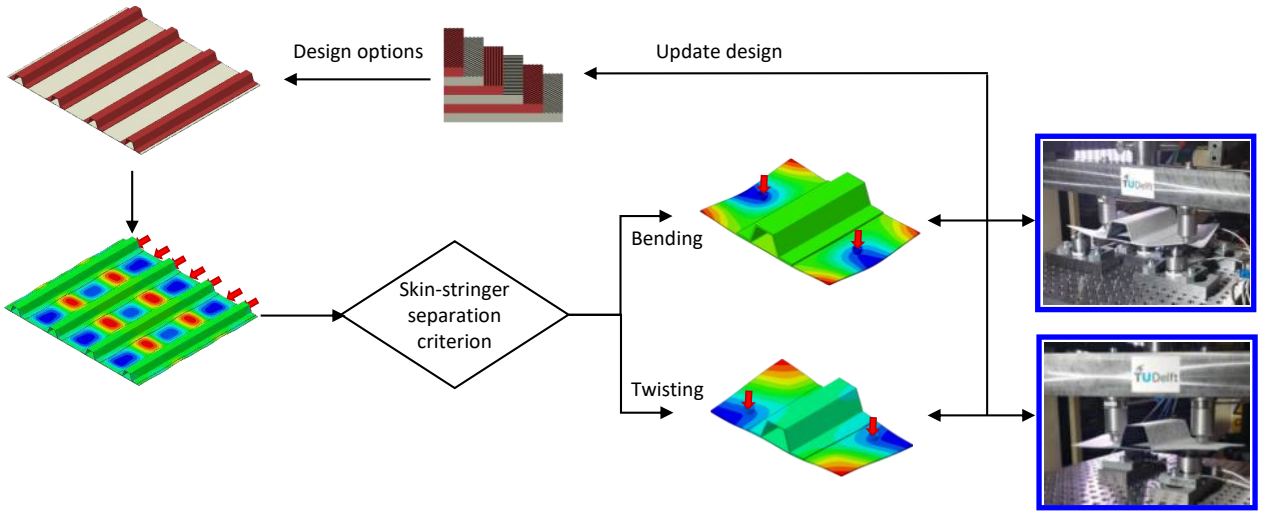

Fig. 1. Flow diagram of proposed methodology.

The methodology requires only the buckling analysis of a multi-stringer panel to identify the critical postbuckling shapes. The critical regions where skin-stringer separation might initiate can be identified using an analytical approach for crack initiation combined with the finite element analysis. With this approach, single-stringer specimens can be designed to represent the critical regions of the multi-stringer panels and reduce the expensive multi-stringer panel testing.

Skin-stringer separation mechanisms and propagation are then studied using finite element models of the single-stringer specimens where the stringer delamination is represented with cohesive elements. The material properties for the skin-stringer interface are obtained from fracture tests of DCB, ENF, and MMB specimens.

The experimental validation is performed using the single-stringer specimens loaded such that they represent the deformation at critical locations on the multi-stringer panel. The single-stringer specimen is tested with loads applied in the out-of-plane direction normal to the skin with supports underneath the skin. The placement of these loading points and support points is designed to reproduce the post-buckling shapes of the multi-stringer panel while inducing damage in a controlled manner. An adaptive multi-point test setup, shown in Fig. 2, is used to provide the different test configurations. With five support points and two loading points, a seven-point bending configuration can replicate the out-of-plane buckling deformation, where the skin tends to bend away from the stringer. With two supports and two loading points in opposing corners, a four-point twisting configuration induces the deformation at the inflection point of the buckling wave, where the skin tends to twist away from the stringer.

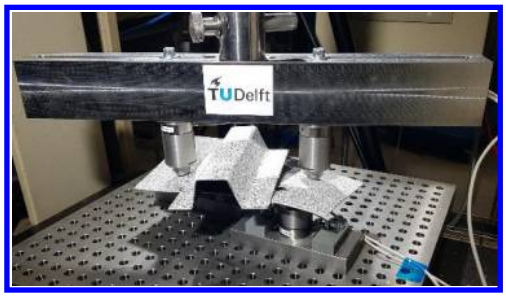

Fig. 2. Single-stringer specimen in the adaptive multi-point test equipment after a four-point twisting configuration test.

The main advantages of the proposed methodology can be summarized as:

- The methodology can be validated using single-stringer specimens representing the multi-stringer panels. The single-stringer specimens are considerably less expensive to test.
- The delamination propagation at the interface of a single-stringer specimen loaded with transverse load points is more stable than in a postbuckled multi-stringer panel and can be measured more easily than in postbuckled panels subjected to in-plane loads [10].
- The shape of the deformation of these single-stringer specimens is imposed by the location of the loading points, so it is not affected by geometrical imperfections nor non-uniformity in the compressive loading distribution.
- The skin-stringer separation due to twisting and bending is investigated in two separate tests, allowing a better understanding of the dominant mode.
- The single-stringer specimens can be used to study different geometrical aspects such as the skin-panel and stringer-flange stacking sequences and the stringer thickness on relatively small numerical models and test specimens.

III. Finite Element Analysis of a Four-Stringer Panel

The first step of the proposed methodology is to develop a finite element model of the multi-stringer panel. The model is used to determine the postbuckling shape and identify the critical areas where skin-stringer separation might occur.

The panel configuration used as a baseline in this research is illustrated in Fig. 3. It consists of four co-cured hat-stringers and is made out of graphite/epoxy IM7/977-3 material [11]. The material properties can be found in Table 1. The panel dimensions are 685 mm in the axial direction, and 770 mm in the width direction. The width of the skin bay between two stringers is approximately 100 mm. The skin of the panel consists of a quasi-isotropic symmetric layup: $[-45/45/0/90/-45/45]_s$. Two stringer designs are considered: a thin layup consisting of $[45/-45/0/90/45/-45]_s$ and a thicker layup: $[45/-45/0/90/45/-45]_{2s}$. The thickness of the panel skin is 1.54 mm, and the thickness of the thin stringer is 1.54 mm while the thick stringer has double the number of plies compared to the thin stringer, resulting in a thickness of 3.07 mm.

The numerical models of the four-stringer panels are developed in Abaqus 2019 [12] using the eight-node continuum shell elements (SC8R). The element size is approximately 2 mm x 2 mm. The two edges of the panel parallel to the stringers are kept unconstrained, whereas the other two edges are clamped. The panel is loaded by applying a compressive displacement in the axial direction.

Table 1. Material properties of IM7/977-3.

Longitudinal modulus	E_{11}	164000	MPa
Transverse modulus	E_{22}	8980	MPa
Shear modulus	G_{12}	5010	MPa
Poisson's ratio	ν_{12}	0.32	
Ply thickness	**t**	0.128	mm
Mode I critical strain energy release rate	G_{IC}	0.256	kJ/m^2

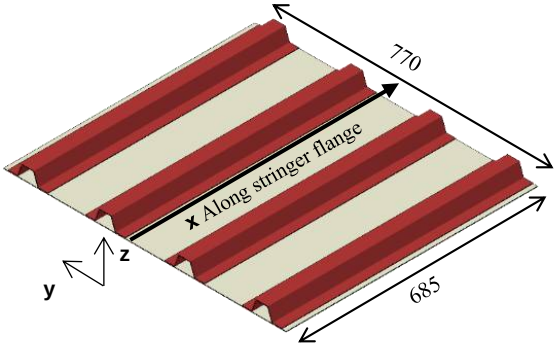

Fig. 3. Four-stringer panel (dimensions in mm).

The force-displacement curves of the two panels are reported in Fig. 4, while the out-of-plane buckling deformation patterns are shown in Fig. 5 at an applied compression displacement of approximately 2.2 mm and 3.4 mm, respectively. The panel with thin stringers presents five buckling half-waves, while the panel with thick stringers has seven half-waves. The out-of-plane deformation of the skin is significantly higher in the panel with thin stringers relative to the panel with thick stringers, even if the applied compression displacement is smaller.

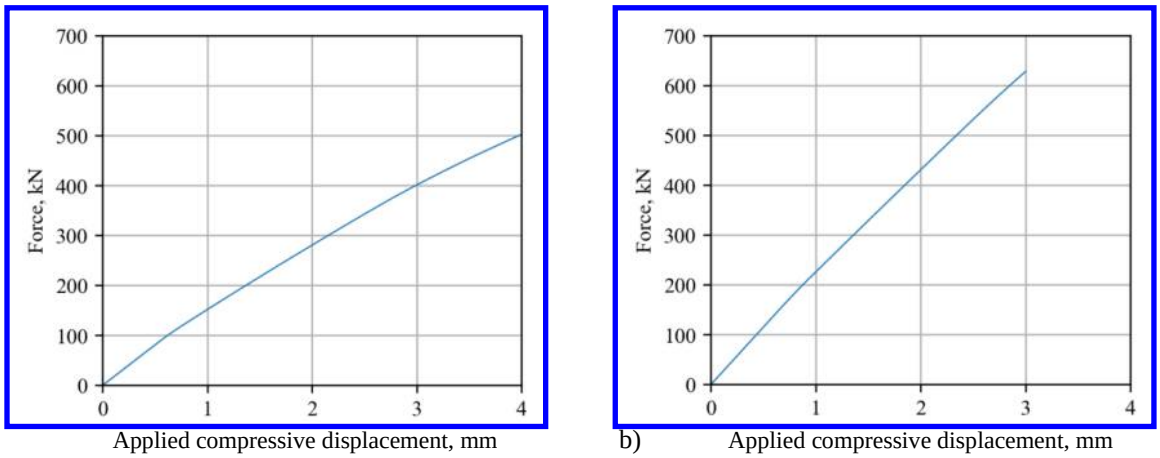

Fig. 4. Force-displacement curves of four-stringer panels: a) panel with thin stringers; b) panel with thick stringers.

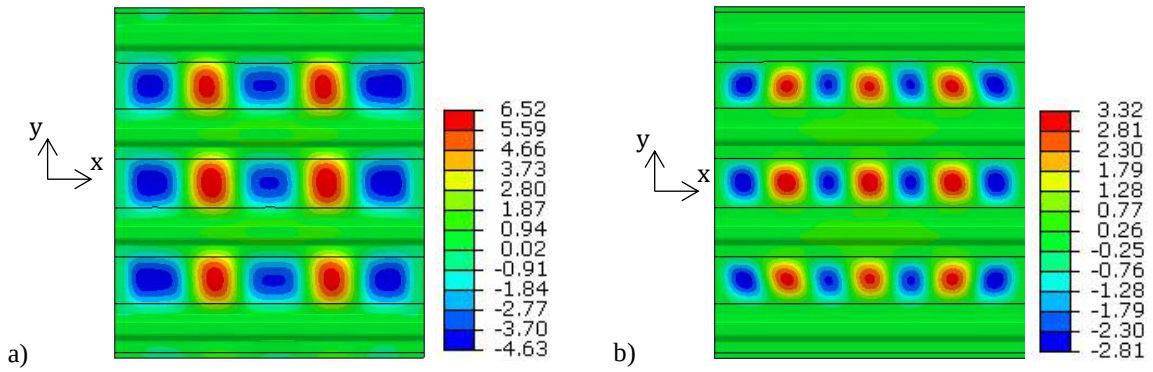

Fig. 5. Postbuckling deformation of four-stringer panels: a) panel with thin stringers at an applied displacement of 3.4 mm; b) panel with thick stringers at an applied displacement of 2.2 mm.

The bending moment and the twisting moment along the stringer edge for the panels with thin and thick stringers are shown in Fig. 6 at applied displacements of 3.4 mm and 2.2 mm, respectively. The moments are taken from the three elements along the flange edge. The blue line labeled s represents the moments in the skin outboard of the flange edge, the line sf1 represents the moments in the skin where the skin and flange overlap, and the line sf2 represents the moments in the flange. In the panel with thin stringers, the twisting moments are significantly higher than the bending moment. The thin panels will likely exhibit skin-stringer separation due to twisting. In the panel with thick stringers the bending moment is significantly high, and this panel will likely exhibit skin-stringer separation due to bending. The bending moment is maximum at the points where the maximum out-of-plane deformation is observed.

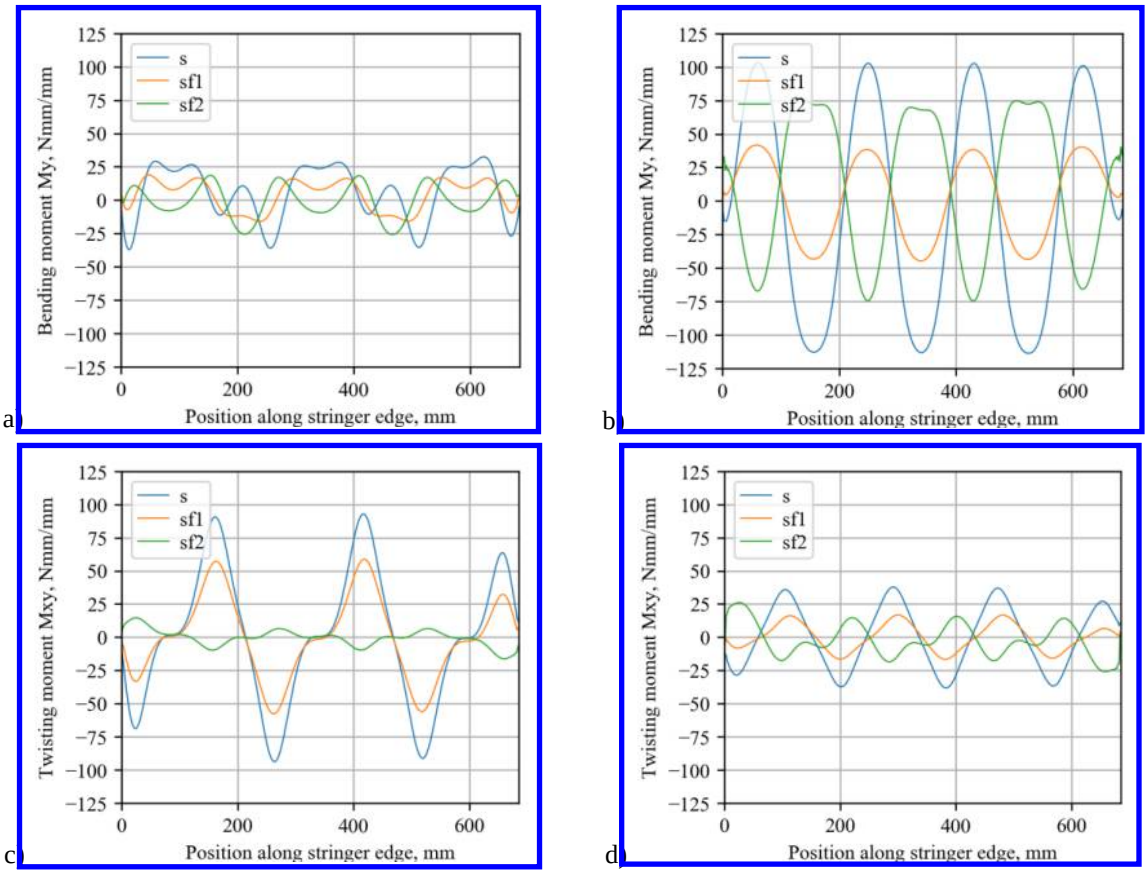

Fig. 6. Bending and twisting moment along flange edge of four-stringer panels: a) Bending moment of panel with thin stringers at applied displacement of 3.4 mm; b) Bending moment of panel with thick stringers at applied displacement of 2.2mm; c) Twisting moment of panel with thin stringers at applied displacement of 3.4 mm; d) Twisting moment of panel with thick stringers at applied displacement of 2.2 mm.

An analytical approach is developed to predict the initiation of skin-stringer separation considering the moments along the skin-flange cross-section. Using the proposed criterion, it is possible to determine at which applied compression displacement and at which location skin-stringer separation occurs, and, depending on the critical mode of separation, the respective single-stringer specimen for bending or twisting is designed, as shown in Fig. 7. When both bending and twisting occur within a close proximity, both specimen configurations are considered.

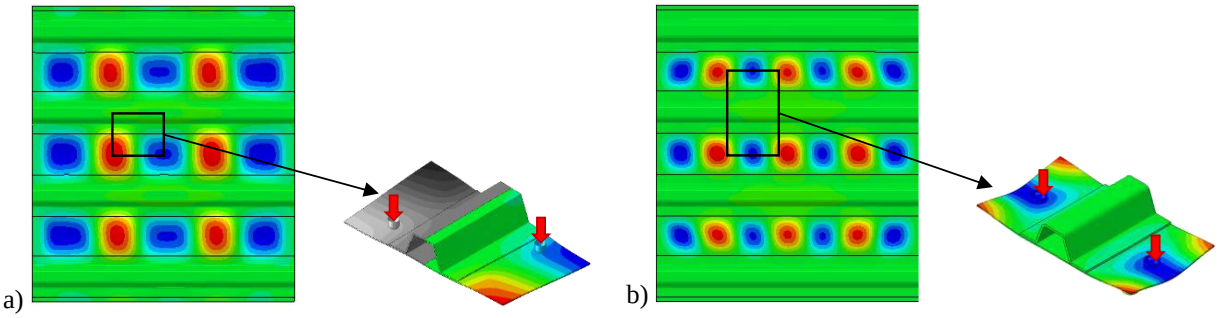

Fig. 7. Configurations of single-stringer specimens for studying multi-stringer panels: a) twisting for panel with thin stringers; b) bending for panel with thick stringers.

IV. Skin-Stringer Separation Criterion

The derivation of the initiation criterion for bending is presented here. This derivation is based on the fracture mechanics-based approach initially developed by Williams [13] to estimate the propagation of an initial crack in laminated composites.

A coupon specimen with an initial pre-crack in a double cantilever beam is used to illustrate the idea, as shown in Fig. 8a. The nomenclature is chosen to designate the top laminate as the flange (f), the bottom laminate as the skin (s) and when these two are connected, the skin-flange overlap as (sf). A moment (M) is applied to the skin, the flange, and the skin-flange overlap and subsequently the different parts undergo a rotation (ϕ). Although the skin-flange overlap is intact, the skin and flange part of the intact overlap are still modeled as separate parts. This is specifically interesting as the slope in the overlap will be bilinear instead of linear. The two connected parts consist of the skin laminate (sf1) and the stringer laminate (sf2).

After a small crack extension, the previous crack front is split into the unconnected skin and flange laminates as can be seen in Fig. 8b. For a small crack extension, it is assumed that the moments in the sections s and f do not change. Hence, the initial moments of the skin and flange now also act on the two unconnected sections at the initial crack front.

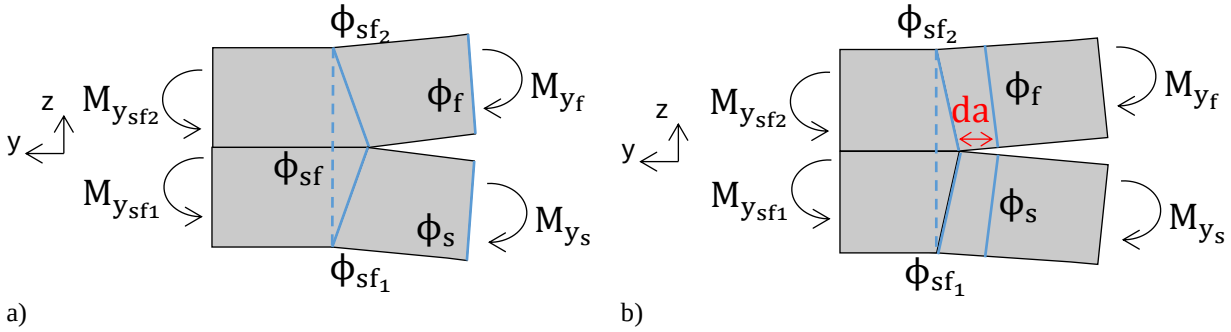

Fig. 8. Skin-flange cross-section: a) initial state; b) after crack propagation.

Due to the small crack extension da, the strain energy (Us) and the external energy (Ue) change and the difference between the two states gives the strain energy release rate (G):

$$G = \left(\frac{dU_e}{da} - \frac{dU_s}{da}\right) \tag{1}$$

The crack extends by a length of da, if the strain energy release rate approaches the critical strain energy release rate (Gc) value. The curvature (κ) in the direction of crack extension is equal to the variation in the slope over the distance dy, therefore:

$$\frac{d\phi}{dy} = \kappa_y = M_y d_{22} \tag{2}$$

where d_{22} is the bending compliance of a composite laminate. The variation in the external energy can be defined as the change in the curvature and applied moment due to the crack extension. The external energy applied to the crack front prior to a crack extension is given by:

$$\frac{dU_e}{da} = \left(M_{y_s}\frac{d\phi_s}{da} + M_{y_f}\frac{d\phi_f}{da}\right) - \left(M_{y_{sf1}}\frac{d\phi_{sf1}}{da} + M_{y_{sf2}}\frac{d\phi_{sf2}}{da}\right) \tag{3}$$

Substituting Eq. 2 and considering that sf1 and s have the same bending compliance and sf2 and f also have the same bending compliance, the following expression is obtained:

$$\frac{dU_e}{da} = \left(M_{y_s}^2 - M_{y_{sf1}}^2\right) d_{22_s} + \left(M_{y_f}^2 - M_{y_{sf2}}^2\right) d_{22_f} \tag{4}$$

The strain energy of a plate subjected to bending moments is given by:

$$U_s = \frac{1}{2} M_y^2 d_{22} \tag{5}$$

Considering the sections at the crack front of Fig. 8a, the following equation is obtained:

$$U_s = \frac{1}{2}\left(M_{y_{sf1}}^2 d_{22_s} + M_{y_{sf2}}^2 d_{22_f}\right) \tag{6}$$

After a crack extension, as represented in Fig. 6b, the strain energy is given by:

$$U_s = \frac{1}{2}\left(M_{y_s}^2 d_{22_s} + M_{y_s}^2 d_{22_f}\right) \tag{7}$$

Therefore, the variation of the strain energy due to the crack extension da is:

$$\begin{aligned}\frac{dU_s}{da} &= \frac{1}{2}\left(M_{y_{sf1}}^2 d_{22_s} + M_{y_{sf2}}^2 d_{22_f}\right) - \frac{1}{2}\left(M_{y_s}^2 d_{22_s} + M_{y_s}^2 d_{22_f}\right) \\ &= \frac{1}{2}\left(M_{y_s}^2 - M_{y_{sf1}}^2\right) d_{22_s} + \frac{1}{2}\left(M_{y_f}^2 - M_{y_{sf2}}^2\right) d_{22_f}\end{aligned} \tag{8}$$

The variation in the strain energy (Eq. 8) is half of the variation in the external energy (Eq. 4), hence the strain energy release rate of Eq. 1 can be written as:

$$G = \frac{1}{2}\left(M_{y_s}^2 - M_{y_{sf1}}^2\right) d_{22_s} + \left(M_{y_f}^2 - M_{y_{sf2}}^2\right) d_{22_f} \tag{9}$$

In the case of the skin-stringer separation, the skin-flange cross-section is illustrated in Fig. 9. In this case a free edge is present where the crack is considered to initiate due to a local moment.

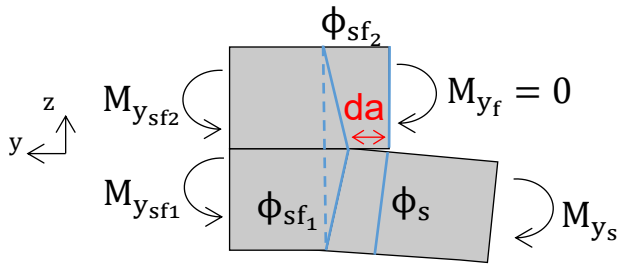

Fig. 9. Skin-flange cross-section with flange termination.

Before a crack extension, the moment in the top section of the skin-flange laminate, sf2, is only attributed to the transfer of the loads from the skin through the skin-stringer interface. This is because there is a free edge and thus My_f is zero. After a crack extension, the moment My_{sf2} becomes zero as well. Therefore, in this case Eq. 9 becomes:

$$G = \frac{1}{2}\left(M_{y_s}^2 d_{22_s} - \left(M_{y_{sf2}}^2 d_{22_f} + M_{y_{sf1}}^2 d_{22_s}\right)\right) \tag{10}$$

The failure index FI that gives the skin-stringer initiation can be calculated by comparing the strain energy release rate to the critical strain energy release rate. Although any stiffness mismatch between skin and flange laminates will couple opening and shear crack tractions, it is assumed that, in the loading case of Fig. 9, the critical strain energy release rate is dominated by mode I. Consequently, the failure index is expressed in terms of the mode I critical energy GIc as:

$$FI = \frac{1}{2G_{Ic}}\left(M_{y_s}^2 d_{22_s} - \left(M_{y_{sf2}}^2 d_{22_f} + M_{y_{sf1}}^2 d_{22_s}\right)\right) \tag{11}$$

The failure index is set to zero if the bending moment is negative in the skin-only section.

V. Application of the Criterion

The criterion is used here to determine the failure index for the skin-stringer separation in the four-stringer panel with thick stringers. The criterion in Eq. 11 and the bending moments obtained by the finite element postbuckling analysis of the panel with thick stringers reported in Fig. 6b are combined as represented in the block-diagram of Fig. 10, to estimate the applied compression displacement and the location of the initiation of the skin-stringer separation.

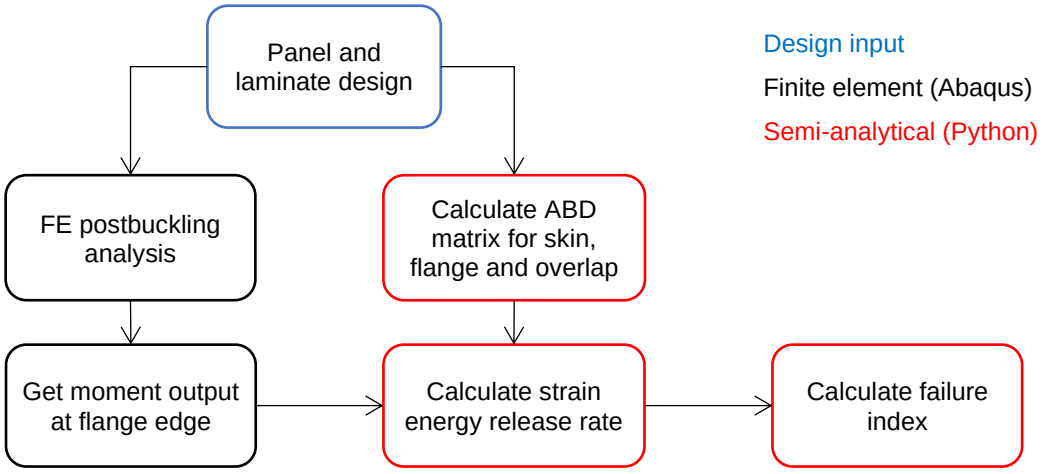

Fig. 10. Block diagram of the developed criterion applied to multi-stringer panels.

The cross-section of the skin-flange overlap of the finite element model is illustrated in Fig. 11. Three element sets are created for each location: s, sf1, and sf2. Every frame of the finite element postbuckling analysis is evaluated, treating each of these sets as a vector with its length equal to the number of elements along the length of the panel.

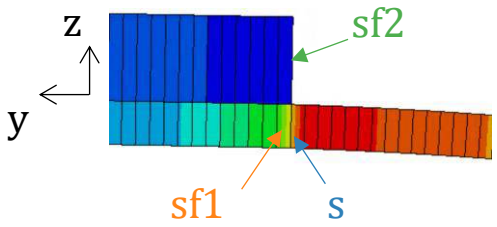

Fig. 11. Cross-section of skin-flange overlap in finite element model.

The failure index is calculated in different sections along the edge of the flange for increased applied compression displacement. The trend at every output frame of the finite element analysis is shown in Fig. 12. It is possible to determine the location and the value of the applied compression displacement in which the failure index is greater than one. The location of the four peaks correspond to the locations of maximum bending. The failure index in the panel with thick stringers exceeded 1 at a displacement of 2.2 mm.

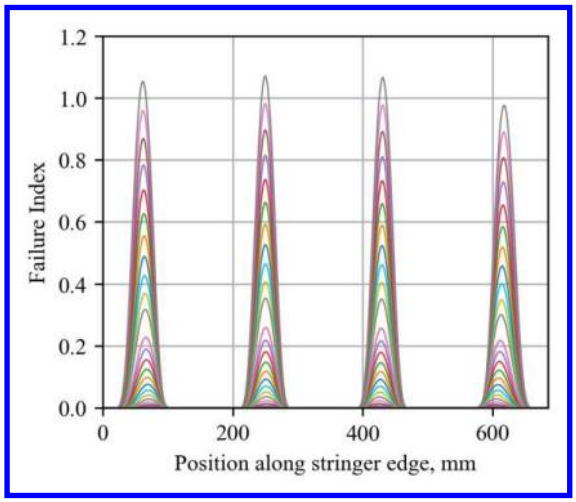

Fig. 12. Failure index due to bending in four-stringer panel with thick stringers.

VI. Single-Stringer Specimen Analysis and Criterion Verification

The criterion highlights the critical region, where skin-stringer separation can initiate. This region is further investigated using a single-stringer specimen in a seven-point bending configuration. The single-stringer specimen can be used to study more in-depth the initiation as well as the propagation of the skin-stringer separation with both finite element analyses and experimental tests.

The single-stringer specimen is chosen such that the buckling deformation of the panel is replicated [9]. The panel length parallel to the stringer is 140 mm while the width is 254 mm. Four supports are placed at a distance of 20 mm from both edges and a fifth support is placed at the center of the specimen. Two loading points are positioned at the center longitudinally, and at 34 mm from the edge of the specimen. The mesh size is 1 mm x 1 mm for the entire specimen.

For verification, the finite element model of the single-stringer specimen is created using cohesive elements at the skin-stringer interface. For the cohesive model a finer mesh is used at the flange region of 0.3 mm x 1 mm. The force-displacement response of the analysis with cohesive elements is given in Fig. 13. At a displacement of 4.8 mm, the first cohesive element reaches a damage variable of 1, which is the point of initiation of skin-stringer separation.

According to the analytical criterion, the failure index is equal to one at an applied displacement of 4.6 mm. The difference between the predicted displacement at skin-stringer separation obtained with the criterion and the analysis with cohesive elements is 4%.

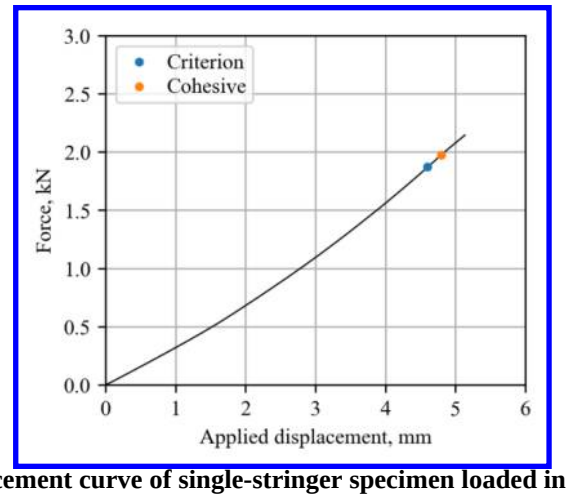

Fig. 13. Force-displacement curve of single-stringer specimen loaded in seven-point bending.

The trend of the bending moments of the single-stringer specimen is compared in Fig. 14 to the trend of the bending moments of the critical area with length equal to 140 mm of the four-stringer panel. In particular, the curves of the bending moments obtained in the skin, s, on the flange of the skin laminate, sf1, and on the stringer laminate, sf2, are reported. For both the single-stringer specimen and the four-stringer panel, the bending moments are taken at the applied displacement where the failure index FI is equal to one. It corresponds to an applied compressive displacement of 4.6 mm for the single-stringer specimen, and to an applied compressive displacement of 2.2 mm for the four-stringer panel.

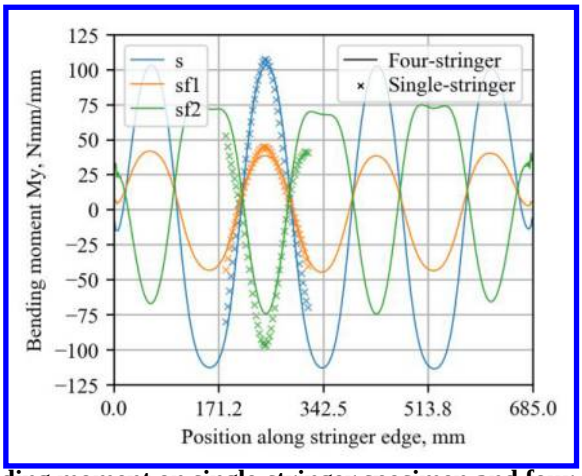

Fig. 14. Bending moment on single-stringer specimen and four-stringer panel.

The bending moment, especially in the skin-only part, is approximately the same for the single-stringer specimen and the four-stringer panel. Specifically, for both cases, it is the bending moment in the skin s that leads to skin-stringer separation. Additionally, the change in the bending moment along the edge of the stringer sf1 is similar between the specimen and the panel. This indicates that presumably, after initiation, the damage propagation in the seven-point bending specimen will be similar to the propagation in the four-stringer panel.

Once validated against the experimental results, single-stringer specimens can be used to perform more detailed evaluations of design details. For instance, design parameters such as skin or stringer thickness or stacking sequence can be optimized using simpler finite element models to increase the load at which skin-stringer separation occurs.

VII. Concluding Remarks

In aeronautical composite stiffened panels, skin-stringer separation is influenced by the buckling response as well as by design parameters such as the skin and stringer thickness and lay-up. A methodology is presented in this paper to understand the interaction between the skin-stringer separation and the postbuckling deformation using single-

stringer specimens. The magnitude of the bending and twisting moment in the skin of a panel can suggest whether skin-stringer separation will occur due to bending or twisting. An analytical criterion was developed for the case of bending to detect at what specific location and at what applied displacement initiation of skin-stringer separation will occur. The propagation of the skin-stringer separation can then be studied using a single-stringer specimen that reproduces the out-of-plane deformation of the postbuckled panel. The similarity between the bending moment along the edge of the single-stringer specimen and that of the four-stringer panel indicates that the single-stringer specimens are useful for verification of the analytical approach. The proposed building block approach facilitates the study of design parameters that might anticipate or delay skin-stringer separation. In a later stage of the design process, the single-stringer specimens can be used to study numerically the propagation of skin-stringer separation and validate the results through a limited number of less expensive tests.

Acknowledgments

The first two authors gratefully acknowledge the financial support received from the European Office of Aerospace Research and Development (EOARD) and the Air Force Research Laboratory of the United States Air Force, under the guidance of Lt. Col. David Garner. Cleared for public release 88ABW-2020-3613.

The authors would like to thank Steven Wanthal of The Boeing Company for sharing his valuable technical experience and his supportive involvement in this research.

References

[1] Bisagni C., and Dávila C.G., "Experimental Investigation of the Postbuckling Response and Collapse of a Single-Stringer Specimen," *Composite Structures*, 108:493-503, 2014.

[2] Minguet P.J., and O'Brien T.K., "Analysis of Test Methods for Characterizing Skin/Stringer Debonding Failures in Reinforced Composite Panels," *Composite Materials: Testing and Design: Twelfth Volume.* ASTM International, 1996.

[3] Van Rijn J.C.F.N., "Design Guidelines for the Prevention of Skin-Stiffener Debonding in Composite Aircraft Panels," NLR Technical Report 2000-355, 2001.

[4] Van Rijn J.C.F.N., and Wiggenraad J.F.M., "A Seven-Point Bending Test to Determine the Strength of the Skin-Stiffener Interface in Composite Aircraft Panels," NLR Technical Report 2000-044, 2000.

[5] Cosentino E., and Weaver P.M., "Approximate Nonlinear Analysis Method for Debonding of Skin/Stringer Composite Assemblies," AIAA Journal, 46(5):1144-1159, 2008.

[6] Falzon B.G., Stevens K.A., and Davies G.O., "Postbuckling Behaviour of a Blade-Stiffened Composite Panel Loaded in Uniaxial Compression," *Composites Part A: Applied Science and Manufacturing*, 31(5):459-468, 2000.

[7] Orifici A.C., Thomson R.S., Herszberg I., Weller T., Degenhardt R., and Bayandor J., "An Analysis Methodology for Failure in Postbuckling Skin-Stiffener Interfaces," *Composite Structures*, 86(1-3):186-193, 2008.

[8] Vescovini R., Dávila C.G., and Bisagni C., "Failure Analysis of Composite Multi-Stringer Panels using Simplified Models," *Composites Part B: Engineering*, 45(1):939-951, 2013.

[9] Kootte L.J., and Bisagni C., "A Methodology to Investigate Skin-Stringer Separation in Postbuckled Composite Stiffened Panels," *Proceedings of the AIAA Scitech 2020 Conference*, 2020.

[10] Leone F.A., Song K., Johnston W., Rose C., Jackson W., and Dávila C.G., "Test/Analysis Correlation of Damage States in Stiffened Post-Buckled Validation Building Block Specimens," *Proceedings of the 34th American Society for Composites Technical Conference*, Atlanta, GA, 23-25 Sept. 2019.

[11] Clay S.B., and Knoth P.M., "Experimental Results of Quasi-Static Testing for Calibration and Validation of Composite Progressive Damage Analysis Methods," *Journal of Composite Materials*, 51(10):1333-1353, 2017.

[12] ABAQUS/Standard User's Manual, Version 2019. Simulia, 2019.

[13] Williams J.G., "On the Calculation of Energy Release Rates for Cracked Laminates", *International Journal of Fracture* 36:101-119, 1988.